Inorganic Chemistry

pubs.acs.org/IC

Article

From +I to +IV, Alkalis to Actinides: Capturing Cations across the Periodic Table with Keggin Polyoxometalate Ligands

Ian Colliard* and Gauthier J.-P. Deblonde*

Cite This: https://doi.org/10.1021/acs.inorgchem.4c02254

Read Online

ACCESS | Metrics & More | Article Recommendations | Supporting Information

ABSTRACT: Coordination chemistry trends across the periodic table are often difficult to probe experimentally due to limitations in finding a versatile but consistent chelating platform that can accommodate various elements without changing its coordination mode. Herein, we present new metal/ligand systems covering a wide range of ionic radii, charges, and elements. Five different ligands derived from the Keggin structure ($HBW_{11}O_{39}^{8-}$, $PW_{11}O_{39}^{7-}$, $SiW_{11}O_{39}^{8-}$, $GeW_{11}O_{39}^{8-}$, and $GaW_{11}O_{39}^{9-}$) were successfully crystallized with six different cations (Na^+, Sr^{2+}, Ba^{2+}, La^{3+}, Ce^{4+}, and Th^{4+}) and characterized by single-crystal X-ray diffraction. Twenty-five new compounds were obtained by using Cs^+ as the counterion, yielding a consistent base formula of $Cs_x[M(XW_{11}O_{39})_2]\cdot nH_2O$. Despite having a similar first-coordination sphere geometry (i.e., 8-coordinated), the nature of the central cation was found to impact the long-range geometry of the complexes. This unique crystallographic data set shows that, despite the traditional consensus, the local geometry of the cation (i.e., metal−oxygen bond distance) is not enough to depict the full impact of the complexed metal ion. The bending and twisting of the complexes, as well as ligand−ligand distances, were all impacted by the nature of the central cation. We also observed that counterions play a critical role by stabilizing the geometry of the $M(XW_{11})_2$ complex and directing complex−complex interactions in the lattice. We also define certain structural limits for this type of complex, with the large Ba^{2+} ion seemingly approaching those limits. This study thus lays the foundation for capturing the coordination chemistry of other rarer elements across the periodic table such as Ra^{2+}, Ac^{3+}, Bk^{4+}, Cf^{3+}, etc.

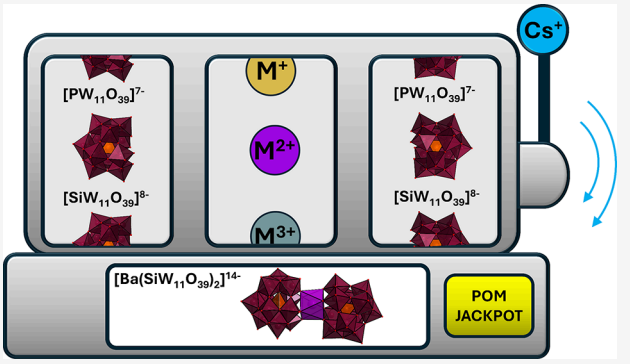

INTRODUCTION

Ever since the first determination of its structure in the 1930s,[1] the Keggin ion ($XW_{12}O_{40}^{n-}$, hereafter XW_{12}) and its derivatives have been extensively studied. Compounds based on the Keggin structure have shown several important applications in catalysis, material sciences, antibacterial drugs, energy storage, computer memory, etc.[2−9] In addition, Keggin ion derivatives and other polyoxometalates (POMs) represent a very diverse class of chelating agents.[10−12] Notable examples include the use of POMs to form luminescent complexes with lanthanide and actinide cations.[13−18] POM chelators offer a set of properties, including high stability, tunable solubility, modular structures, and controllable coordination geometries, that cannot be readily accessed with common chelators, making them useful tools for a wide variety of metal-based applications.[19−22]

Likewise, classic chelators, such as simple inorganic oxoanions (NO_3^-, SO_4^{2-}, and PO_4^{3-}) or organic ligands (carboxylates, porphyrins, siderophores, peptides, etc.), have also been extensively used as metal chelators in various fields, including medicine, environmental science, and industrial processes.[23−30] These more traditional chelators are typically light (with M < 1000 g/mol, e.g., EDTA) or sufficiently flexible to accommodate the coordination preferences of 6- or 8-coordinated metals ions within the d-block and f-block (Zn^{2+}, Fe^{3+}, $Ln^{4+/3+}$, and $An^{4+/3+}$).[31−37] However, most of these ligands tend to form simple salts rather than actual metal/ligand complexes with monovalent alkali and divalent alkaline earth ions (Na^+, Cs^+, Sr^{2+}, and Ba^{2+}) and instead simply precipitate the cations for charge balancing, without strong coordination with the cation. As a result, specific chelators have been developed for large and soft cations such as Cs^+, Ba^{2+}, and, more recently, even Ra^{2+} and Ac^{3+}.[38−43] These specific chelators are designed to provide 9−12 coordinating atoms, enough to accommodate the large coordination sphere of the alkali and alkaline earth ions but too high for the 6-coordinated d-block or 8-coordinated f-block cations. As a result, for series of metal/chelator systems with traditional chelators, changes in the cation's coordination number, metal:chelator ratio, or chelator's binding mode are

Received: May 30, 2024
Revised: August 13, 2024
Accepted: August 16, 2024

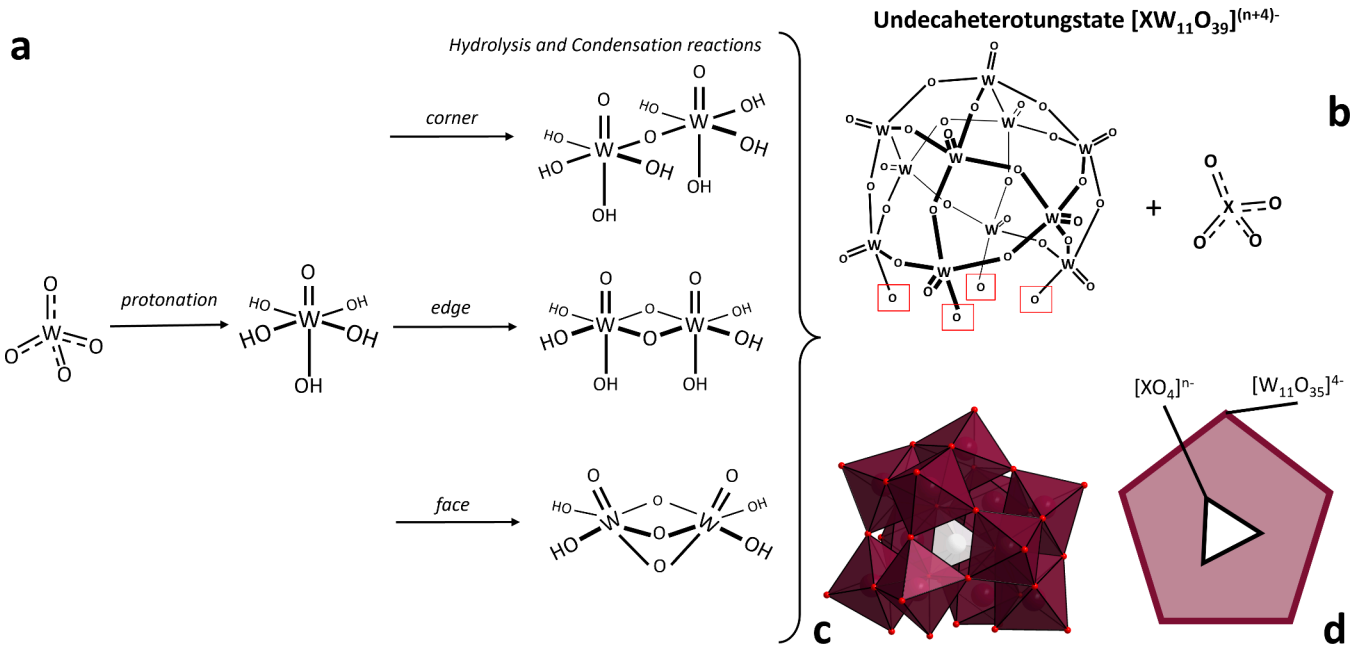

Figure 1. Description of the reactions leading to the structure of the lacunary and tungsten-based Keggin ion $[XW_{11}O_{39}]^{n-}$ (XW_{11}). (a) Building units, conversion, and three hydrolysis and condensation reactions that yield polyoxotungstates. (b) Emphasis on the tetrahedral heteroatoms (X) that can be incorporated into the Keggin structure. In this study, X = B, P, Si, Ge, or Ga. (c) Polyhedral representation of XW_{11}, with tungsten colored maroon, oxygen shown as red spheres, and the heteroatom colored white. (d) Simplified projection of XW_{11} with the maroon pentagon representing the $[W_{11}O_{35}]^{4-}$ cage and the white triangle representing the tetrahedral heteroanion (XO_4^{n-}) encapsulated in the Keggin structure. See Figure S1 for a detailed view of the different bonds in the Keggin structure.

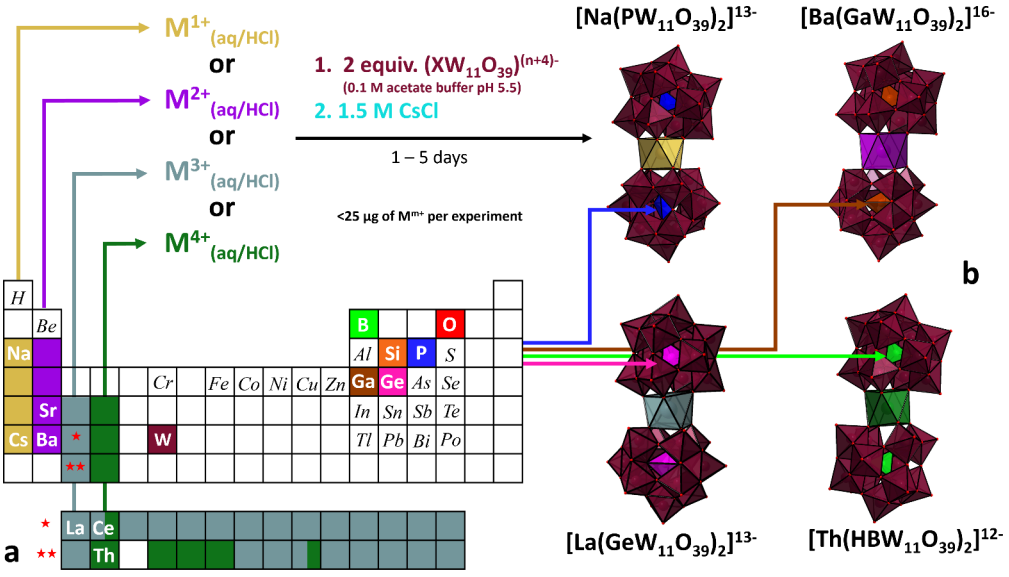

Figure 2. Summary of the elements that are compatible with the Keggin structure. (a) Periodic table showing elements (colored) studied herein. Italicized elements can be incorporated into the XW_{11} Keggin structure as XO_4. Monovalent cations are colored yellow, divalent cations purple, trivalent cations blue-gray, and tetravalent cations green. All cations under the same synthesis conditions are bound to XW_{11}, where X = B (light green), Si (orange), P (blue), Ge (pink), or Ga (brown). WO_6 polyhedra are colored maroon. (b) Select structures highlighting the variety of compositions and charges. For more information about the structures reported in this study, see Tables S1–S6.

often observed when going from large and soft cations (e.g., Na^+ and Ba^{2+}) to small and hard ones (e.g., $Ln^{4+/3+}$ and $An^{4+/3+}$).[44−50]

Under these circumstances, it is difficult to evaluate binding trends across the periodic table, because multiple variables change concurrently. We here attempted to fill this gap by searching for a chelating platform that allows for the synthesis and characterization of metal:ligand coordination compounds in a consistent and comparable manner, without major changes in the first coordination sphere of the complexed metal ion. We focused on the Keggin structure[1] as a potential universal chelating platform that provides a consistent coordination framework, with the goal of directly comparing the coordination chemistry of a broad range of cations across the periodic table, going from monovalent alkalis to tetravalent actinides. On the basis of our prior work on POM complexes with heavy trivalent

https://doi.org/10.1021/acs.inorgchem.4c02254
Inorg. Chem. XXXX, XXX, XXX−XXX

Table 1. Summary of the Cations and Polyoxometalate (POM) Ligand Complexes Reported in This Work[a]

		$[HBW_{11}O_{39}]^{8-}$	$[PW_{11}O_{39}]^{7-}$	$[SiW_{11}O_{39}]^{8-}$	$[GeW_{11}O_{39}]^{8-}$	$[GaW_{11}O_{39}]^{9-}$
		0.11[c]	0.17[c]	0.26[c]	0.39[c]	0.47[c]
Na^{+}	1.180[b]	√	√	√	‡	‡
Sr^{2+}	1.260[b]	√	√	√	√	√
Ba^{2+}	1.420[b]	‡	√	√	√	√
La^{3+}	1.160[b]	√	√	√	√	√
Ce^{4+}	0.970[b]	√	√	√	√	√
Th^{4+}	1.105[b]	√	√	√	√	‡

[a]Check marks indicate the cation/POM systems for which we obtained at least one single-crystal XRD structure. Double daggers indicate that no crystal formation was observed (see Results amd Discussion). We recently reported the structure of the $La^{3+}/PW_{11}O_{39}^{7-}$ system elsewhere.[52] [b]Ionic radii (angstroms) of the 8-coordinated cations. [c]Ionic radii (angstroms) of the 4-coordinated heteroelements in the Keggin structure (B^{3+}, P^{5+}, Si^{4+}, Ge^{4+}, and Ga^{3+}). Ionic radii were taken from Shannon's seminal review.[63]

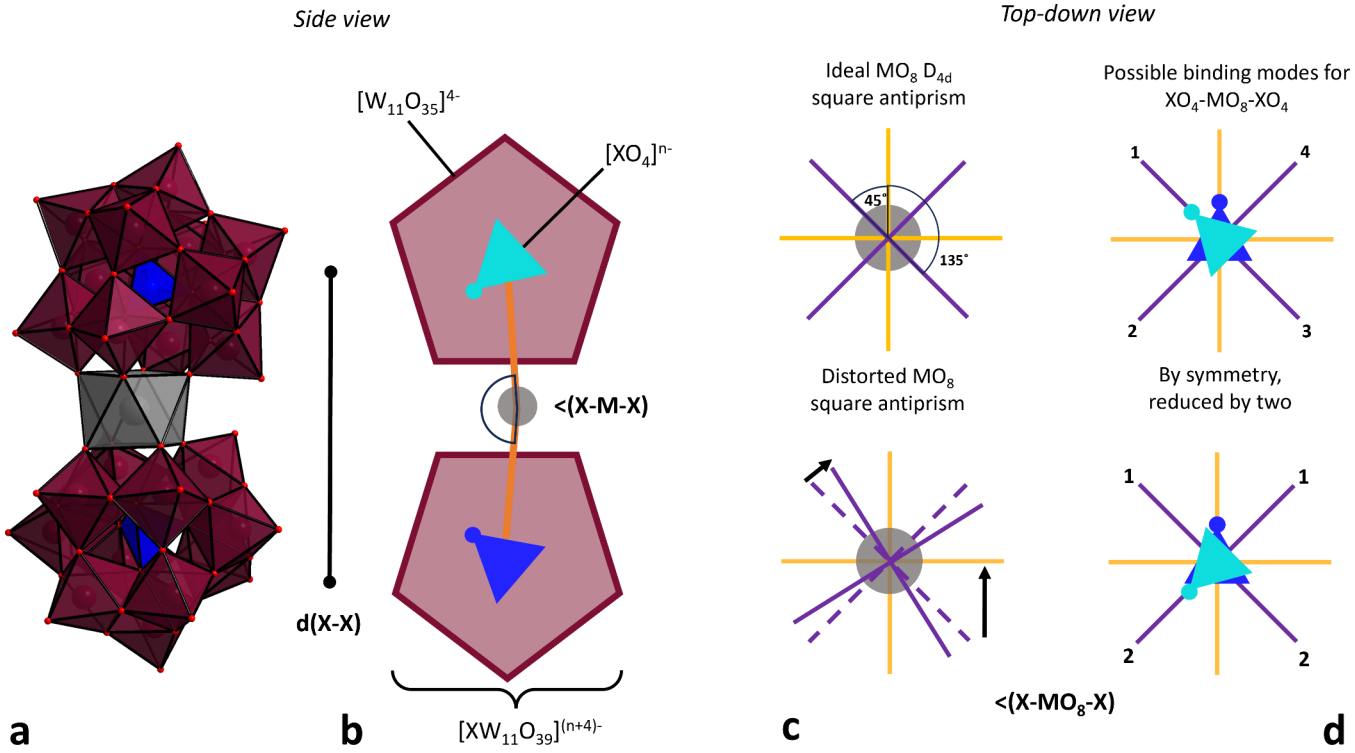

Figure 3. Visual schematic of the structural parameters related to the Keggin complexes. (a) Polyhedral representation of $M(POM)_2$, with W shown as a maroon polyhedral, oxygen as red spheres, and central metal M^{m+} as a gray polyhedron. (b) Simplified side view projection of $M(POM)_2$, with W shown shown as a maroon pentagon and the central tetrahedral heteroatom as blue triangles (light and dark). d(X–X) is the distance between the triangles, and ∠(X–MO_8–X) is the angle between the triangles and the central metal ion (surrounded by eight oxygens from the POM). (c) Top-down view representation showing only the central M^{m+} ion as a gray sphere and the yellow and purple lines representing its eight bonds. The deviation from ideal symmetry is shown. (d) Top-down and simplified view focusing on the two heteroatoms in the $M(XW_{11}O_{39})_2$ complex and their four different possible positions relative to each other, which are reduced to two possible combinations at 45° and 135°. For numerical values of M–O distances, d(X–X), ∠(X–MO_8–X), and ∠(X–MO_8–X), see Table S7. For a three-dimensional view of the torsion of the POM complexes, see Figure S2.

actinides,[17,18,51,52] we selected tungsten-based Keggin ligands. The Keggin ions used in this study for cation complexation are derived from the parent Keggin structure $XW_{12}O_{40}^{n-}$ (where X = P, B, Al, etc.).[1] Careful pH control yields stable and isolable derivatives, often fragments or aggregates of the parent structure.[6,10] These derivatives are labeled as "lacunary polytungstates", of which $[\alpha\text{-}XW_{11}O_{39}]^{(n+4)-}$ (abbreviated as XW_{11}) has been the most readily studied structure since it was first reported in 1966.[53] The XW_{11} structure (Figure 1) occurs by removing a single [WO] unit from the parent structure[1] $XW_{12}O_{40}^{n-}$, at pH >1.5. Because of the tetrahedral symmetry of the parent structure, any [WO] unit that is removed yields the same XW_{11} lacunary Keggin ion. XW_{11} can be seen as a $[W_{11}O_{35}]^{4-}$ open cage that surrounds a $[XO_4]^{n-}$ anion (Figure 1b–d). The XW_{11} structure makes up arguably the most diverse and largest class of lacunary polyanions, and it can seemingly incorporate any tetrahedral $[XO_4]^{n-}$ anion. Several examples of heteroelements have been incorporated into the Keggin structure, with the most readily isolable being the ones containing B^{3+}, Si^{4+}, P^{5+}, Ga^{3+}, or Ge^{4+}.[54−57] More complex synthesis procedures[53,58] and the use of stabilizing elements have also led to Keggin ions XW_{11} for which X = Be^{2+}, Al^{3+}, S^{4+}, Cr^{3+}, $Co^{2+/3+}$, Ni^{2+}, Cu^{2+}, Zn^{2+}, As^{5+}, Sb^{5+}, or Bi^{5+} (Figure 2). This likely represents the most versatile small molecule structure in which various heteroelements can be encapsulated and

https://doi.org/10.1021/acs.inorgchem.4c02254
Inorg. Chem. XXXX, XXX, XXX−XXX

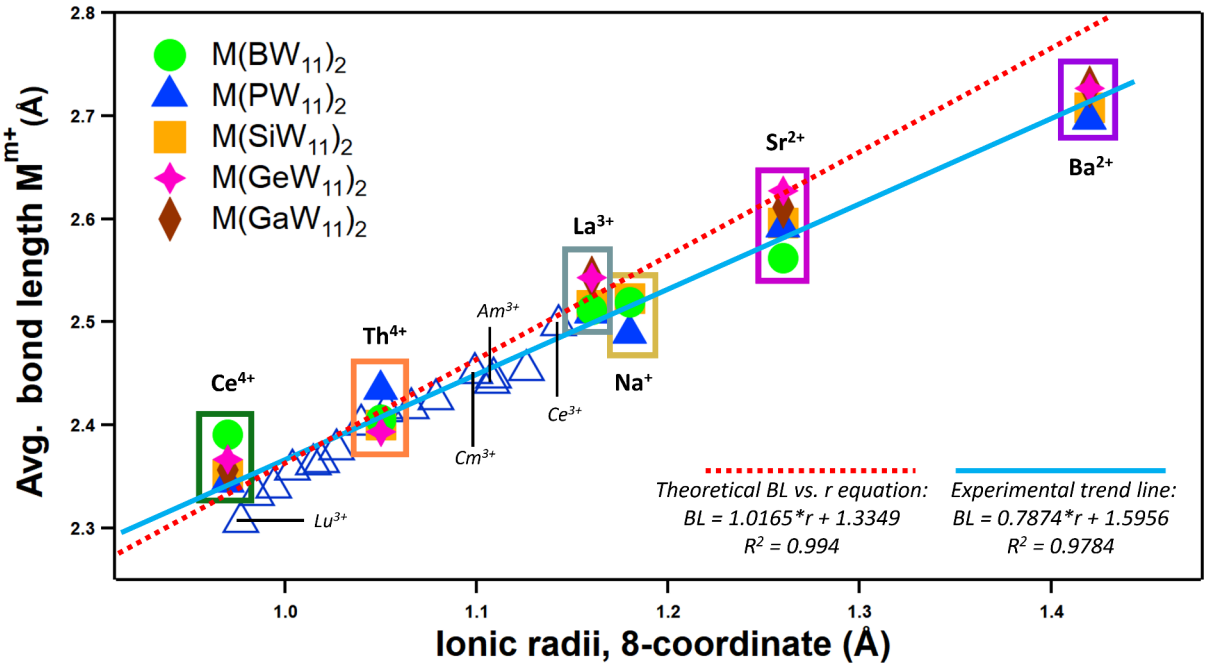

Figure 4. Average M−O^{POM} bond lengths (BLs) for the 25 new Keggin structures obtained in this work. The *x*-axis corresponds to the ionic radii of central metal M^{m+} within the base formula $Cs_{(m+2n+8)}[M(XW_{11}O_{39})_2]^{(m+2n+8)-}$. M = Na^+ (yellow box), Sr^{2+} (pink box), Ba^{2+} (purple box), La^{3+} (gray box), Ce^{4+} (green box), or Th^{4+} (orange box). The empty blue triangles represent the bond lengths for trivalent actinides and lanthanides in the isotypic An/Ln$(PW_{11})_2$ compounds; we recently reported the corresponding crystal structures in separate studies.[17,52] The solid blue line represents the experimental trendline for M−O bond lengths, for all M$(XW_{11})_2$ compounds displayed in this figure. The dashed red line represents theoretical bond lengths based on bond valence sum parameters. For more information, see Tables S7 and S8.

eventually used as an integral part of a water-soluble ligand for cation complexation.

Isolation of an XW_{11} chelator (X = B, Si, P, Ga, or Ge) provides unique synthesis opportunities. With the removal of a [WO] unit from the parent XW_{12}, four oxygens become exposed and reactive (Figure 1b). If cations are present in solution, then XW_{11} can essentially act as a tetradentate ligand, forming complexes such as $[M(XW_{11}O_{39})(H_2O)_n]^{x-}$ and $[M(XW_{11}O_{39})_2]^{y-}$.[17,51,59] In prior work, first-row transition metals and trivalent lanthanides have been bound to XW_{11} (X = B, Si, P, Ga, or Ge) (Figure 2a). More recently, BW_{11} and PW_{11} have also been shown, through microscale crystallization techniques, to bind to and crystallize with trivalent heavy actinides Am/Cm$(PW_{11})_2$.[17,51,52] Complexes of Keggin ions Zr^{4+}, Ce^{4+}, and U^{4+} have also been reported,[60−62] but those compounds often contain different counterions or have been obtained under readily different conditions, impeding comparison. Thus far, there has been no systematic study of the chelating ability of the Keggin ion for cations and heteroelements across the periodic table.

Herein, we report 25 new single-crystal structures based on five different lacunary Keggin ligands, XW_{11} ($[HBW_{11}O_{39}]^{8-}$, $[PW_{11}O_{39}]^{7-}$, $[SiW_{11}O_{39}]^{8-}$, $[GeW_{11}O_{39}]^{8-}$, and $[GaW_{11}O_{39}]^{9-}$), binding to six different M^{m+} cations (Na^+, Sr^{2+}, Ba^{2+}, La^{3+}, Ce^{4+}, and Th^{4+}) with a wide variety of charges and ionic radii (Table 1). The resulting complex series displays a wide range of overall charge (from −16 to −10) and structural diversity, while keeping the first-coordination sphere geometry of the central cation as 8-coordinated. This study shows that POMs can be used as a consistent and practical chelating platform to study ions across the periodic table, from soft monovalent alkalis to hard tetravalent lanthanides and actinides.

RESULTS AND DISCUSSION

Structural Description and Metrics. All compounds reported here were synthesized and crystallized in the same manner. We used our microscale approach that we developed for the chemistry of transplutonium elements[17,18,52] and extend here. Briefly, a CsCl aqueous solution (6 M) is titrated into a 75 μL drop of a 100 μM solution of the targeted M$(XW_{11})_2$ complex, in 100 mM acetate buffer at pH 5.5 (see the Experimental Section and the Supporting Information for additional details). Single crystals suitable for X-ray diffraction studies grew within approximately 24−120 h. The M$(XW_{11})_2$ structures reported here share a consistent base formula of $Cs_{(m+2n+8)}[M(XW_{11}O_{39})_2]^{(m+2n+8)-}$, where two $XW_{11}O_{39}^{n-}$ ligands chelate a central cation M^{m+} in the +I, +II, +III, or +IV oxidation state. The central cation is bound in an eight-coordinate environment, with all cases (Table 1) featuring a square antiprismatic geometry [except Na$(BW_{11})_2$ (cubic geometry)]. To the best of our knowledge, this represents the first system of its kind capable of crystallizing cations of a broad range of sizes and charges (monovalent alkalis, divalent alkaline earths, trivalent and tetravalent lanthanides, and actinides) in the same local coordination environment. The consistent syntheses and crystallization minimize variables, creating conditions for more suitable comparisons.

Due to the wide range of crystal structures reported (Table 1), morphological trends can be studied as a function of both the heteroatom within the XW_{11} ligand and the central cation. For all of the structures reported herein, a select number of variables effectively change with respect to the central metal ion (Figure 2).

A traditional and widely used morphological parameter to analyze metal/ligand complexes is the metal−oxygen bond length. We defined three additional parameters to analyze

https://doi.org/10.1021/acs.inorgchem.4c02254
Inorg. Chem. XXXX, XXX, XXX−XXX

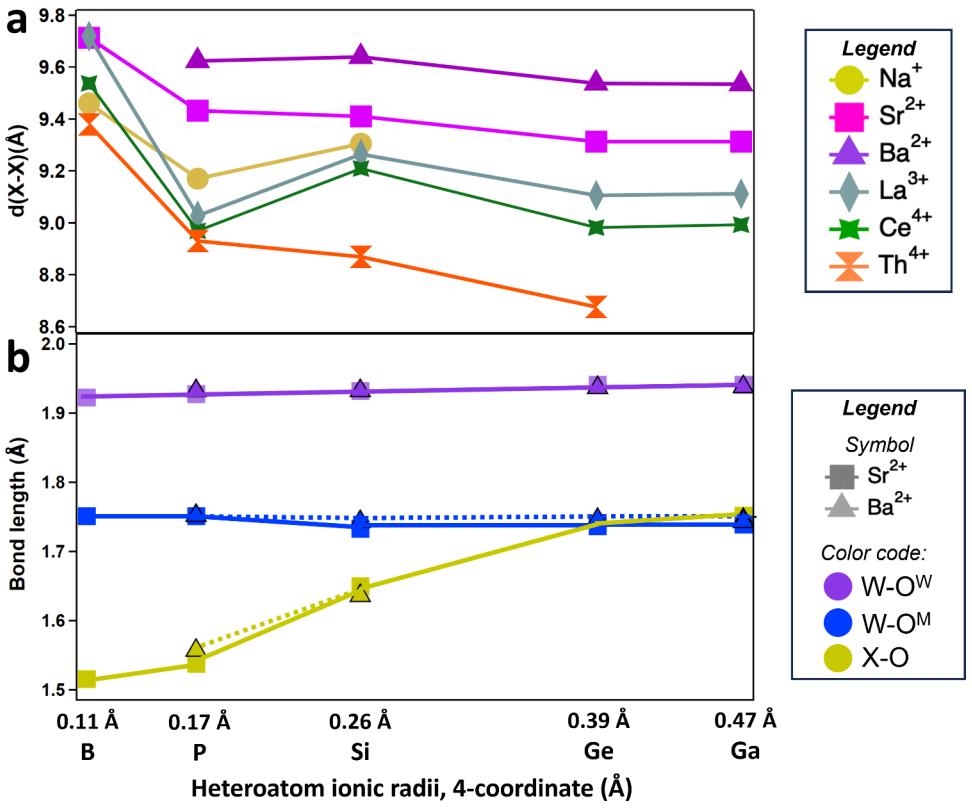

Figure 5. Relevant distances related to the $M(XW_{11}O_{39})_2$ structures. (a) Distances, d(X−X), between the heteroelements, X, of the two POM ligands within the $M(XW_{11}O_{39})_2$ structures. (b) Comparison of the average bond lengths for the Sr^{2+} (solid lines) and Ba^{2+} (dotted lines) complexes. X-O represents the average bond length between the heteroelement X and oxygens within the XO_4^{n-} anion encapsulated within $XW_{11}O_{39}^{x-}$. W−O^W represents the average tungsten−oxygen bond length for oxygens bound to tungstens. W−O^M represents the average tungsten−oxygen bond length for the eight oxygens bound to the central cation.

structural trends across the 25 new metal/ligand compounds reported herein (Figure 3). The first parameter we defined is the angle created between the two encapsulated $[XO_4]$ ions within the two XW_{11} ligands and the central M^{m+}, denoted ∠(X−M−X), where M = Na^+, Sr^{2+}, Ba^{2+}, La^{3+}, Ce^{4+}, or Th^{4+}. The second parameter of interest is the distance between the two XW_{11} ligands, using the X in the central anion XO_4^{n-} inside the POM, denoted d(X−X). The third defined parameter is the torsion angle between the two sets of four oxygens around the central cation, denoted ∠(X−MO_8−X). This measures the deviation from the perfect D_{4D} symmetry for the square antiprismatic coordination of M^{m+} in relation to the tetrahedral heteroatom. Because there are two possible ideal positions at 45° and 135° (Figure 3c,d), the torsion is taken as the absolute value of the angle between the positions. As discussed hereafter, these structural parameters are impacted by the nature of the central cation and are telltale signs of the long-range arrangement of the overall structures.

First Coordination Sphere of the Central Cation and Structural Limits for Keggin Complexes. For most metal/ligand complexes, one could expect a strong correlation between the ionic radius of the metal and the metal−oxygen distances of the metal's first coordination sphere. The five $M(XW_{11})_2$ POM systems studied here follow this trend, and we could confirm an almost perfectly linear correlation, from the large Ba^{2+} to the small Ce^{4+} (Figure 4). Similar PW_{11} complexes that we previously isolated[17,S2] with the trivalent lanthanides (La to Lu, except Pm) and Am^{3+} and Cm^{3+} complexes also fit this trend.

The M−O bond length range for Ba^{2+} [ionic radius (IR) of 1.420 Å for 8-coordination[63]], averaged over the five different POMs, is 2.696−2.728 Å with a standard deviation (SD) of 0.015 Å. For Sr^{2+} (IR = 1.260 Å[63]), the range is 2.562−2.627 Å (SD of 0.024 Å). For Na^+ (IR = 1.180 Å[63]), the range is 2.489−2.531 Å (SD of 0.022 Å). For La^{3+} (IR = 1.120 Å[63]), the range is 2.508−2.544 Å (SD of 0.017 Å). For Ce^{4+} (IR = 0.970 Å[63]), the range is 2.344−2.391 Å (SD of 0.020 Å). For Th^{4+} (IR = 1.050 Å[63]), the range is 2.394−2.434 Å (SD of 0.016 Å) (Figure 4). Average bond distances and additional crystallographic metrics are listed in Tables S7 and S8. Among the structures, there is a small standard deviation, indicating low variability in the first coordination sphere of the cation among the five different Keggin ligands studied here, despite them containing different heteroelements and having different charges (Table 1).

Through bond valence summations, further comparisons can be performed to validate the central cation valency. Calculations on all M^{m+}/O^{POM} systems revealed consistent and expected oxidation states. For Na^+, the calculated valency ranged from 1.093 to 1.208. For Sr^{2+}, it ranged from 1.979 to 2.267. For Ba^{2+}, it ranged from 2.306 to 2.493. For La^{3+}, it ranged from 2.743 to 3.021. For Th^{4+}, it ranged from 3.761 to 4.137. For Ce^{4+}, it ranged from 3.396 to 3.856 (Table S8). While the calculated valency values are close to the expected values, Ba^{2+} is the only cation that shows significant and consistently higher-than-expected valency for the five POM systems. This implies that the measured bond lengths are shorter than anticipated for Ba^{2+}, as shown in Figure 4. When considering the POM−POM distance (Figure 5a), the d(X−X) value for $Sr(POMs)_2$ and $Ba(POMs)_2$

https://doi.org/10.1021/acs.inorgchem.4c02254
Inorg. Chem. XXXX, XXX, XXX−XXX

increases by only ~0.20 Å [e.g., from 9.432 to 9.624 Å for PW_{11} and from 9.411 to 9.639 Å for SiW_{11} (Figure 5)], i.e., only ~70% of the expected lengthening due to the increase in the radius between those two ions [+0.16 Å from Sr^{2+} to Ba^{2+}, hence expected increase of ~0.32 Å for d(X−X)]. We presume that these deviations arise from overbonding of the Ba^{2+} ion (i.e., stronger electron donation from the POM to Ba^{2+}, resulting in shorter-than-expected Ba−O distances and a higher calculated oxidation state for Ba^{2+}, based on bond valence sum calculations). In terms of what may cause overbonding, and with only one accessible oxidation state in solution (i.e., +II), we hypothesize that the barium ion's size might be reaching the limits of the Keggin structure.

The presence of a large Ba^{2+} at the center of the complex, combined with the presence of large Cs^{+} counterions for charge balancing, may also create steric hindrance, preventing the crystallization of some of the POM complexes with Ba^{2+}. Among the five XW_{11} POMs studied, the boron derivative is the one that leads to the longest d(X−X) distances, yet with some of the shortest M−O bond lengths (Figures 5a and 4). Interestingly, Ba^{2+} did not crystallize with BW_{11}. On the basis of the other reported structures, extrapolation for a hypothetical $Ba(BW_{11})_2$ would yield a d(X−X) of >10 Å (Figure 5a), yet with a Ba−O bond length of 2.669 Å, which is too short for Ba^{2+} (Figure S3 and Table S9). This suggests that Ba^{2+} is likely too large to form a complex with BW_{11}. Attempts to crystallize PW_{11} and BW_{11} complexing an 8-coordinated Cs^{+} also failed. As such, it is probable that even larger cations (e.g., Cs^{+}, Ra^{2+}, and Ac^{3+}) may not be able to form the same $M(BW_{11})_2$ structures as those reported here.

The SiW_{11} ligand may also not be optimal for these larger cations, also having long POM−POM distances (Figure 5a). On the contrary, the crystallization of Ce^{4+} shown here and Zr^{4+} (with PW_{11} and alkylamine counterions, reported by Kato et al.[64]) implies that there is a reasonable assurance that the five POMs studied here can also complex and crystallize transuranic ions (Np^{4+}, Pu^{4+}, $Bk^{3+/4+}$, and Cf^{3+}) as their ionic radii fit within the range shown in Figure 4. These cases will be evaluated in subsequent studies.

Bending, Stretching, and Twisting of Metal/POM Complexes. When considering the other structural parameters defined above for the $M(POM)_2$ complexes (Figure 3), subtle yet increasingly divergent behaviors are observed for each XW_{11} and each central cation (Figures 5 and 6). Such compounding differences are then later reflected in the lattice arrangement of $M(XW_{11})_2$ (Figure 7).

The first trend to consider here, which is counterintuitive, is the general decrease in d(X−X) with an increase in heteroelement size (Figure 5a). For example, the BO_4^{5-} anions within the $M(BW_{11})_2$ complexes are located farther from the central cation than GaO_4^{5-} of the $M(GaW_{11})_2$ complexes, despite Ga^{3+} being ~4.5 times larger than B^{3+} (tetrahedral ionic radii of 0.47 and 0.11 Å, respectively).[63] As shown in Figure 5b, the size of the encapsulated anion increases in the following order: BO_4^{5-} > PO_4^{3-} > SiO_4^{4-} > GeO_4^{4-} > GaO_4^{5-}. This is reflected in the measured X−O distances with the $M(XW_{11})_2$ complexes. However, the W−O bonds within the complexes are unaffected when heteroelement X is changed. Given these observations, it is thus reasonable to conclude that the $[W_{11}O_{35}]^{4-}$ "cage" is fairly rigid, with the $[XO_4]^{n-}$ and $[MO_8]$ species becoming the subtle structural directors.

The PW_{11} series emerges as the most divergent among all of the structures described here. Except for $M^{II}(PW_{11})_2$ (M = Sr^{2+} or Ba^{2+}), the d(X−X) values of the PW_{11} structures are shorter than those of BW_{11} and SiW_{11} (Figure 5a). The next most noticeable trend, where PW_{11} exhibits divergent behavior, is the bending angle between the heteroatoms, ∠(X−M−X) (Figure 6a). The $M(PW_{11})_2$ (M = Na^{+}, La^{3+}, or Ce^{4+}) complexes feature the smallest bending angle (161.5−166.7°). The other PW_{11} compounds, $Ba(PW_{11})_2$ and $Sr(PW_{11})_2$, and all of the other $M(XW_{11})_2$ structures [except $Th(SiW_{11})_2$] have larger angles of 176.0−180.0°. When considering the torsion angle, ∠(X−MO_8−X) (Figure 6b) and considering the ideal positions at 45° and 135° (Figure 3d and Table S7), even more unique behavior is observed for PW_{11}. $Na(BW_{11})_2$, $Na(PW_{11})_2$, $La(PW_{11})_2$, $Ce(PW_{11})_2$, $Th(PW_{11})_2$, $Th(SiW_{11})_2$, and $Th(GeW_{11})_2$, bind at an angle of 45°. All of the other reported structures (Table 1) feature square antiprismatic coordination with the 135° position. Considering all of the structures reported here, a clearer relationship between the torsion and bending of the complexes emerges. Structures featuring a strong bending [i.e., ∠(X−M−X) of <170°] also display a larger torsion angle [i.e., ∠(X−MO_8−X) of 45° preferred over 135°]. Taking this step further, we found that the structures with larger bending and torsion angles feature shorter distances between the heteroatoms, d(X−X). This relationship in turn can be seen to affect the long-range positions of the cesium counterions surrounding the $M(XW_{11})_2$ structures, affecting the lattice arrangement of the whole structure, as described hereafter.

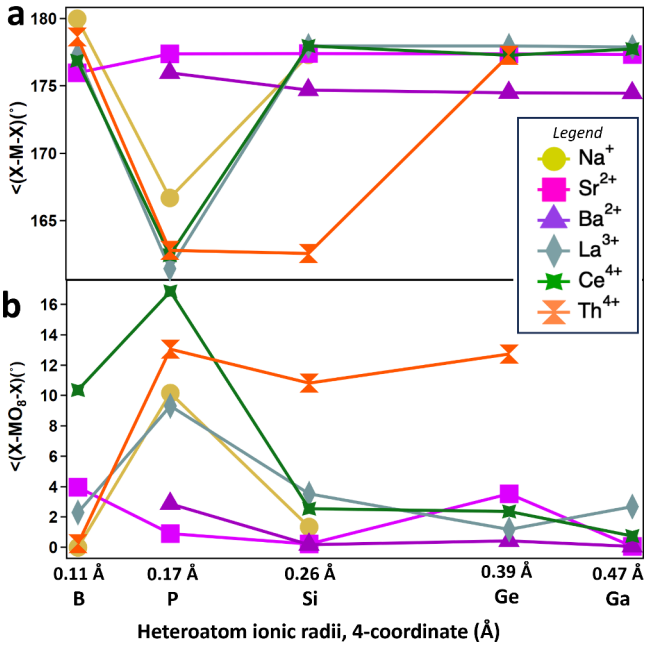

Figure 6. Bending and twisting angles related to the $M(XW_{11}O_{39})_2$ structures. (a) Bending angle between XW_{11} ligands and the central metal, ∠(X−M−X). (b) Torsion angle of XW_{11}, ∠(X−MO_8−X). See Figure 3 for a definition of the morphological parameters. The x-axis is sorted by the increasing size of the heteroatom.

Long-Range Structure and Unsuspected but Critical Role of Counterions. Extending perspectives beyond the minutia of metal/ligand complex geometry, we found that Cs^{+} counterions directly impact the lattice arrangements the complexes form. Counterions have previously been shown to impact significantly the solubility of POMs, notably for alkalis via ion-pair formation.[21,65] We also recently observed the formation of the rare β isomer of the Keggin structure[66] for Cm^{3+} upon crystallization with PW_{11} and cesium as the

https://doi.org/10.1021/acs.inorgchem.4c02254
Inorg. Chem. XXXX, XXX, XXX−XXX

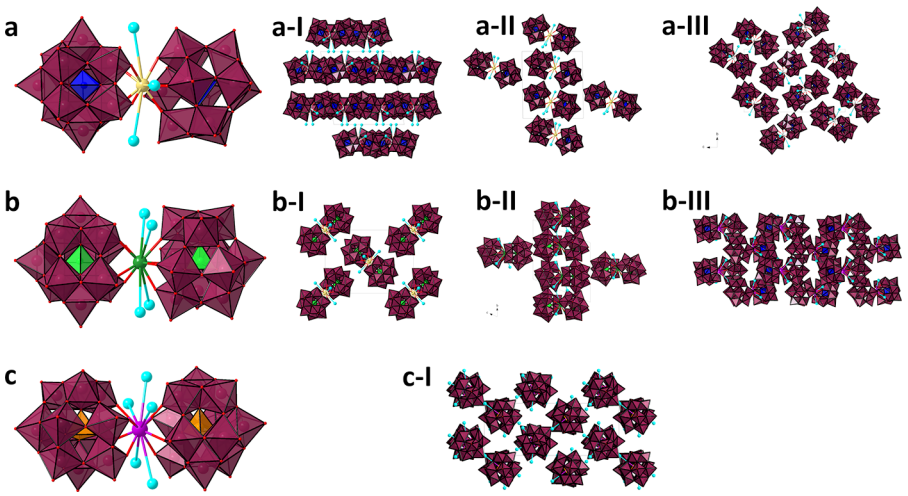

Figure 7. Equatorial Cs counterions and framework types observed among the $Cs_xM(PW_{11}O_{39})_2$ compounds. (a and a-I–a-III) Three equatorial Cs counterions and three lattice types. (b and b-I–b-III) Four equatorial Cs counterions and three lattice types. (c and c-I) Five equatorial Cs counterions and only one lattice type. Framework type a-I is encountered with only $M(PW_{11})_2$, where Ln = Am^{3+}, Y^{3+}, and Eu^{3+}–Lu^{3+}. We reported this specific framework type in a recent study.[52] Additional visualizations of the structures are shown in Figures S5–S11.

counterion, hinting at the potential non-innocent role of counterions in POM complexes.[17,52] In the study presented here, only the α isomer of the Keggin structure was observed, regardless of the central cation.

Because all of the structures obtained here with Na^+, Sr^{2+}, Ba^{2+}, La^{3+}, Ce^{4+}, and Th^{4+} follow the same base formula of $Cs_{(m+2n+8)}[M(XW_{11}O_{39})_2]^{(m+2n+8)-}$, the series allows for a consistent analysis of the impact of Cs^+ in such complexes.

In broad terms, there are seven frameworks that feature complexes stacking either parallel or perpendicular to each other (panel a vs panel b of Figure 7 and Table 2). Each of these seven

Table 2. Analysis of the Long-Range Organization with the $Cs_xM(PW_{11}O_{39})_2$ Compounds Studied Here

	Na^+	Sr^{2+}	Ba^{2+}	La^{3+}	Ce^{4+}	Th^{4+}
			Framework Type[a]			
$[HBW_{11}O_{39}]^{8-}$	b-I	c-I		b-III	b-II	c-I
$[SiW_{11}O_{39}]^{8-}$	c-I	c-I	b-III	c-I	c-I	a-II
$[PW_{11}O_{39}]^{7-}$	a-II	b-III	b-III	a-II	a-II	a-III
$[GaW_{11}O_{39}]^{9-}$		c-I	b-III	c-I	c-I	
$[GeW_{11}O_{39}]^{8-}$		c-I	b-III	c-I	b-II	a-II
			Number of equivalent Cs^+ for POM			
$[HBW_{11}O_{39}]^{8-}$	4	5		4	4	5
$[SiW_{11}O_{39}]^{8-}$	5	5	4	5	5	2
$[PW_{11}O_{39}]^{7-}$	3	4	4	3	3	3
$[GaW_{11}O_{39}]^{9-}$		5	4	5	5	
$[GeW_{11}O_{39}]^{8-}$		5	4	5	4	2

[a]For the number of surrounding or equatorial cesiums with the corresponding framework formations, see Figure 7. See Figure S4 for the volume of the complexes taken into account in the calculation of charge densities.

lattices can be subdivided further when considering the role of the Cs^+ counterions. When considering only fully occupied Cs^+, at positions closest to the central cation (because they will have the strongest impact on the structure), we consistently observe three to five Cs^+ cations <5.5 Å from the central cation. Other Cs^+ cations are more than ~7 Å distant. The Cs–O bond lengths consistently fall in the range of 2.968–3.554 Å, and the Cs^+ ions exhibit a 12–14 coordination environment. This set of Cs counterions will be termed "equatorial Cs^+". Table 2 summarizes the seven lattice types and the number of equatorial Cs atoms observed for all of the structures. For structures with five Cs atoms, only one lattice type was observed. For structures with four and three equatorial Cs atoms, three lattice types were observed (Figure 7 and Figures S5–S11).

A correlation between the morphological parameters (Figure 3) and the number of Cs^+ cations arises when compared to the torsion and bending angles. Structures that featured a large torsion or bending angle [e.g., $Na(PW_{11})_2$, $La(PW_{11})_2$, and $Ce(PW_{11})_2$] have the fewest equatorial Cs^+ species (i.e., three). The structures that have the smallest torsion or bending angle [e.g., $Sr(SiW_{11})_2$] have all five Cs atoms. One would expect the distance between the two POM ligands, d(X–X), to have the strongest effect on the number of Cs counterions, as a smaller d(X–X) would leave less room for the Cs counterions. The $Ba(XW_{11})_2$ structures, with their large Ba^{2+} central ion, reveal as much and display d(X–X) values 0.220 Å longer than those of their Sr^{2+} counterparts. However, the $Ba(XW_{11})_2$ structures maintain smaller torsion and bending angles.

To understand the role that Cs^+ plays in lattice formation, we can also correlate the charge of the complexes to the morphological parameters, as structural parameters alone cannot explain the different lattices for the same number of equatorial Cs^+ cations. More specifically, it is important to consider the charge of the complex normalized by the "volume" of the complex. For the reported structures, the smaller the d(X–X) parameters, the smaller the overall volume for the complex (see Table S10 and Figure S4 for geometric proof). As such, comparing complexes becomes easier when their charge density is considered.

The impact of local complex geometry on the long-range lattice becomes greater if the $M(XW_{11})_2$ complexes feature longer d(X–X) distances and/or higher charges; then, the complex will feature lattices that minimize complex–complex interactions by maximizing the number of equatorial Cs atoms. For example, for the Th^{4+} series, d(X–X) is 9.379 Å for $[Th(HBW_{11})_2]^{12-}$, 8.931 Å for $[Th(PW_{11})_2]^{10-}$, 8.870 Å for $[Th(SiW_{11})_2]^{12-}$, and 8.676 Å for $[Th(GeW_{11})_2]^{12-}$. As such, because $Th(BW_{11})_2$ has the longest d(X–X), it features five equatorial Cs atoms and a lattice arrangement in which the

https://doi.org/10.1021/acs.inorgchem.4c02254
Inorg. Chem. XXXX, XXX, XXX–XXX

complexes are stacked staggered to each other (Figure 7c-I), which maximizes the distance between complexes (i.e., minimizes complex−complex interactions). For equally charged complexes $[Th(SiW_{11})_2]^{12-}$ and $[Th(GeW_{11})_2]^{12-}$, they have significantly smaller d(X−X) values, which leads to a higher charge density (Table 2). Their lattice arrangement for these complexes is different from that for $[Th(HBW_{11})_2]^{12-}$ but also minimizes complex−complex interactions (Figure 7a-III). For $[Th(PW_{11})_2]^{10-}$, which has d(X−X) values comparable to those of Si and Ge but has the lowest charge density of all of the $Th(XW_{11})_2$ complexes, its lattice exhibits complexes "pairs" that are arranged in a perpendicular manner, thus maximizing complex−complex interactions. From these experimental structures, we can establish the roles of the Cs counterions. They stabilize the geometry of the $M(XW_{11})_2$ complex and tune the complex−complex interactions to accommodate the size and charge of the cation/POM complexes. In future studies, it would be interesting to investigate whether the correlations between the charge density and the position of the alkali cations observed here across many Keggin complexes also apply to other types of lacunary POMs, such as the Well−Dawson structure.

CONCLUSION

This study presents a large number of new metal/ligand complexes involving POM ligands derived from Keggin ions. Five different Keggin ions ($HBW_{11}O_{39}^{8-}$, $PW_{11}O_{39}^{7-}$, $SiW_{11}O_{39}^{8-}$, $GeW_{11}O_{39}^{8-}$, and $GaW_{11}O_{39}^{9-}$) were successfully crystallized and characterized with six different cations (Na^+, Sr^{2+}, Ba^{2+}, La^{3+}, Ce^{4+}, and Th^{4+}). Twenty-five new compounds were obtained by using Cs^+ as a counterion, yielding a consistent base formula of $Cs_{(m+2n+8)}[M^{m+}(XW_{11}O_{39})_2]^{(m+2n+8)-}$. Despite the broad range of elements and ionic radii involved in those compounds, all of the central cations studied here feature a similar 8-coordinated environment, sandwiched by the two tetradentate POM ligands. This allows for a direct and broad scope comparison of the chemistry of various elements across the periodic table.

The unique crystallographic data set reported here shows that, despite the historical consensus, the local geometry of the cation (i.e., metal−oxygen bond distance) is not enough to reflect the full impact of the cation on the structure. Across the 25 new compounds reported here, a strong and predictable linear correlation was observed between metal−oxygen bond distances and the ionic radii of the central cation. However, structural diversity manifested well beyond the first coordination sphere of the central cation. The bending and twisting of the complexes as well as the POM−POM distance were found to vary significantly depending on the central cation. Furthermore, the counterion (in this case Cs^+) was found to provide an extra layer of structural diversity in the reported structures. While counterions are generally considered to be spectators in chemical reactions, the Cs^+ ions were found to be a convenient magnifying tool of the impact of the central cation on the structure. Depending on the nature of the central cation and its subtle impact on the local geometry, Cs^+ counterions were found to stabilize the geometry of $M(XW_{11})_2$ and direct complex−complex interactions to accommodate the size and charge of the $M(XW_{11})_2$ complexes. We thus establish that the size of the central cation directs the local geometry more effectively than the charge, whereas the overall charge of the complex and Cs^+ ions directs the lattice formations. Finally, the large cation Ba^{2+} (and Cs^+) seems to be approaching the limit of the Keggin complexes, being unable to crystallize with $HBW_{11}O_{39}^{8-}$. This study, combined with our approach recently developed to crystallize POM compounds at the microscale,[17] thus lays the foundation for examining more extreme and rarer ions of the periodic table, such as Ra^{2+}, Ac^{3+}, Bk^{4+}, Cf^{3+}, etc.

EXPERIMENTAL SECTION

Materials. Metal chlorides (alkalis, alkali earths, and lanthanides), thorium chloride, ammonium cerium nitrate, sodium acetate, cesium chloride, sodium tungstate dihydrate, phosphoric acid, sodium metasilicate, germanium oxide, gallium nitrate, and sodium borate were purchased from chemical providers (VWR and Millipore Sigma) and used as received. All solutions were prepared using deionized water purified by a reverse osmosis cartridge system (≥18.2 MΩ cm). All experiments were performed in a temperature-controlled room (22 °C).

Caution! *^{232}Th and most of its decay products constitute serious health hazards because of their radioactive and chemical properties. All experiments involving radionuclides were conducted at Lawrence Livermore National Laboratory, in facilities designed for the safe handling of long- and short-lived radioactive materials and associated waste.*

Crystallographic Studies. All M/POM structures were collected using a Rigaku Synergy Custom single-crystal diffractometer, equipped with a κ goniometer and using Mo Kα radiation (λ = 0.71073 Å) with a full width at half-maximum of ∼200 μm at the sample from a MicroMax-007 HF microfocus rotating anode source. Images were recorded on a Dectris Pilatus 3R (300 K, CdTe) detector and processed using CrysAlisPro. After integration, both analytical absorption and empirical absorption (spherical harmonic, image scaling, and detector scaling) corrections were applied.[40] All structures were determined by the intrinsic phasing method from SHELXT,[41] developed by successive difference Fourier syntheses, and refined by full-matrix least squares on all F2 data using SHELX42 via the OLEX2 interface.[43] Crystallographic information for the six reported structures can be obtained free of charge from the Cambridge Crystallographic Data Center (https://www.ccdc.cam.ac.uk/) upon referencing CCDC numbers in the crystallographic tables.

Synthesis. The corresponding metal chloride salts (or nitrate salt for Ce) were in 0.1 M HCl. The corresponding POM was dissolved to make a 200 μM solution. A stoichiometric amount of the M^{m+} stock solution was added to the POM solution to obtain a 1:2 metal:POM ratio. X-ray diffraction (XRD)-quality crystals were then mounted and characterized, while the rest were characterized by Raman microscopy (see the Supporting Information for detailed syntheses).

POM Nomenclature. The borate derivative of the Keggin structure is the only one that is protonated under the studied conditions. For the sake of simplicity and consistency with the other Keggin ligands used in this study, we chose to abbreviate them as XW_{11} (e.g., PW_{11} and BW_{11}) but give the protonation state when the full formula is mentioned (e.g., $PW_{11}O_{39}^{7-}$ and $HBW_{11}O_{39}^{8-}$).

Undecaborotungstate (BW_{11}) Complexes. The metal/undecaborotungstate complex series is based on the $[\alpha$-$HBW_{11}O_{39}]^{8-}$ (BW_{11}) lacunary Keggin ligand. In the series of Keggin ions studied, BW_{11} is the only one that is protonated.[67] It was demonstrated through solution-state ^{17}O and ^{183}W nuclear magnetic resonance (NMR) spectroscopy experiments that the smaller size and higher charge for B^{III} lead to a shift in its stability window to "lower" pH values.[67] As such, the only derivative stable at pH <7 is protonated $[H_xBW_{11}O_{39}]^{x-9}$, which is consistent with our crystallography results. Note that the proton is located on the tungsten scaffold and not on the encapsulated borate ion, BO_4^{3-}. Under the synthesis conditions reported in this study, BW_{11} binds and crystallizes with Na^+, Sr^{2+}, La^{3+}, Ce^{4+}, and Th^{4+}, but not with Ba^{2+}. Across the four $M(BW_{11})_2$ structures reported here, there are a range of average bond lengths of 1.510−1.520 Å for the B−O bond, 2.380−2.385 Å for the W−O^x bond, 1.832−2.085 Å for the W−O^c bond, and 1.618−1.757 Å for the W−O^t bond (see Figure S1 for oxygen designation within XW_{11}). $Na(BW_{11})_2$, fully formulated as $Cs_{15}Na(HBW_{11}O_{39})_2{\cdot}2H_2O$, crystallizes in monoclinic space group $P2_1/n$ with a V of 4680.3(3) Å^3. It is noteworthy that the $Na(BW_{11})_2$ crystal is the only structure reported here that features a cubic coordination

https://doi.org/10.1021/acs.inorgchem.4c02254
Inorg. Chem. XXXX, XXX, XXX−XXX

environment for the Na^+ ion, as opposed to the square antiprismatic geometry encountered for the others. $Sr(BW_{11})_2$, formulated as $Cs_{14}Sr(HBW_{11}O_{39})_2{\cdot}9H_2O$, crystallizes in monoclinic space group $P2_1/n$ with a V of 9738.2(3) Å. $La(BW_{11})_2$, formulated as $Cs_{13}La(HBW_{11}O_{39})_2{\cdot}H_2O$, crystallizes in monoclinic space group $P2_1/n$ with a V of 9650.5(3) Å^3. $Ce(BW_{11})_2$, formulated as $Cs_{12}Ce^{IV}(HBW_{11}O_{39})_2{\cdot}12H_2O$, crystallizes in triclinic space group $P\bar{1}$ with a V of 4562.1(11) Å. $Th(BW_{11})_2$ fully formulated as $Cs_{12}Th(HBW_{11}O_{39})_2{\cdot}11H_2O$ crystallizes in monoclinic space group $P2_1/n$ with a V of 9595.6(3) Å^3. While the H atom could not be found directly through SCXRD, the charge of all structures was confirmed by freely refining the Cs^+ ions, and converging to the final value reported (for more information about refinement, see the Supporting Information and Table S1). The M−O bond distances are also consistent with the charge of the central cation. Interestingly, no crystal formation was observed for Ba^{2+} and $[HBW_{11}O_{39}]^{8-}$ (see Results and Discussion).

Undecasilicotungstate (SiW_{11}) Complexes. The $M(SiW_{11})_2$ series is based on the $[\alpha\text{-}SiW_{11}O_{39}]^{8-}$ lacunary Keggin. Cations Na^+, Ba^{2+}, Sr^{2+}, La^{3+}, Ce^{4+}, and Th^{4+} bound and crystallized with this silico Keggin ion under synthesis conditions similar to those described above. Across the reported structures, there are a range of average bond lengths of 1.628−1.650 Å for the Si−O bond, 2.326−2.338 Å for the W−O^x bond, 1.789−2.027 Å for the W−O^c bond, and 1.611−1.746 Å for the W−O^t bond.

$Na(SiW_{11})_2$, formulated as $Cs_{15}Na(SiW_{11}O_{39})_2{\cdot}11H_2O$, crystallizes in monoclinic space group $P2_1/n$ with a V of 9716.2(2) Å^3. $Sr(SiW_{11})_2$, formulated as $Cs_{14}Sr(SiW_{11}O_{39})_2{\cdot}H_2O$, crystallizes in monoclinic space group $P2_1/n$ with a V of 9886.8(4) Å. $Ba(SiW_{11})_2$, formulated as $Cs_{14}Ba(SiW_{11}O_{39})_2{\cdot}6H_2O$, crystallizes in monoclinic space group $P2_1/n$ with a V of 9866.5(4) Å^3. $La(SiW)_{11}$, formulated as $Cs_{13}La(SiW_{11}O_{39})_2{\cdot}14H_2O$, crystallizes in monoclinic space group $P2_1/n$ with a V of 9764.5(4) Å^3. $Ce(SiW_{11})_2$, formulated as $Cs_{12}Ce^{IV}(SiW_{11}O_{39})_2{\cdot}15H_2O$, crystallizes in monoclinic space group $P2_1/n$ with a V of 9753.9(19) Å^3. $Th(SiW_{11})_2$, fully formulated as $Cs_{12}Th(SiW_{11}O_{39})_2{\cdot}13H_2O$, crystallizes in monoclinic space group $P2_1/n$ with a V of 4850.0(4) Å^3. See Table S2 for more information.

Undecaphosphotungstate (PW_{11}) Complexes. The $M(PW_{11})_2$ series is based on the $[\alpha\text{-}PW_{11}O_{39}]^{7-}$ lacunary Keggin and can bind to the same cations mentioned above, Na^+, Sr^{2+}, La^{3+}, Ce^{4+}, and Th^{4+}, under similar synthesis conditions. Across the reported structures, there are a range of average bond lengths of 1.531−1.563 Å for the P−O bond, 2.401−2.436 Å for the W−O^x bond, 1.844−2.066 Å for the W−O^c bond, and 1.618−1.758 Å for the W−O^t bond.

$Na(PW_{11})_2$, formulated as $Cs_{13}Na(PW_{11}O_{39})_2{\cdot}11H_2O$, crystallizes in monoclinic space group $P2_1/n$ with a V of 5327.4(14) Å^3. $Sr(PW_{11})_2$, formulated as $Cs_{12}Sr(PW_{11}O_{39})_2{\cdot}H_2O$, crystallizes in monoclinic space group $P2_1/n$ with a V of 9827.5(5) Å^3. $Ba(PW_{11})_2$, formulated as $Cs_{12}Ba(PW_{11}O_{39})_2{\cdot}6H_2O$, crystallizes in monoclinic space group $P2_1/n$ with a V of 9918.3(6) Å^3. $La(PW_{11})_2$, previously published,[S2] formulated as $Cs_{11}La(PW_{11}O_{39})_2{\cdot}9H_2O$, crystallizes in monoclinic space group $P2_1/n$ with a V of 4377.1(4) Å^3. $Ce(PW)_{11}$, formulated as $Cs_{10}Ce^{IV}(PW_{11}O_{39})_2{\cdot}5H_2O$, crystallizes in monoclinic space group $P2_1/n$ with a V of 4679.7(2) Å^3. $Th(PW_{11})_2$, fully formulated as $Cs_{10}Th(PW_{11}O_{39})_2{\cdot}9H_2O$, crystallizes in monoclinic space group $P2_1/n$ with a V of 8908.4(15) Å^3. See Table S3 for more information.

Undecagallotungstate (GaW_{11}) Complexes. The $M(GaW_{11})_2$ series is based on $[\alpha\text{-}GaW_{11}O_{39}]^{9-}$ lacunary Keggin. The following cations, Sr^{2+}, La^{3+}, Ce^{4+}, and Th^{4+}, complexed and crystallized under synthesis conditions similar to those described above. Across the reported structures, there are a range of average bond lengths of 1.731−1.752 Å for the Ga−O bond, 2.280−2.307 Å for the W−O^x bond, 1.853−2.050 Å for the W−O^c bond, and 1.633−1.734 Å for the W−O^t bond.

$Sr(GaW_{11})_2$, formulated as $Na_2Cs_{14}Sr(GaW_{11}O_{39})_2{\cdot}H_2O$, crystallizes in monoclinic space group $P2_1/n$ with a V of 9881.4(3) Å^3. Curiously, it is the only structure crystallizing with a mix of Na and Cs counterions [excluding the reported $Na(XW_{11})_2$ complexes reported here]. $Ba(GaW_{11})_2$, formulated as $Cs_{16}Ba(GaW_{11}O_{39})_2{\cdot}5H_2O$, crystallizes in monoclinic space group $P2_1/n$ with a V of 9862.9(2) Å^3. $La(GaW_{11})_2$, formulated as $Cs_{15}La(GaW_{11}O_{39})_2{\cdot}15H_2O$, crystallizes in monoclinic space group $P2_1/n$ with a V of 9858.3(5) Å^3. $Ce(GaW_{11})_2$, formulated as $Cs_{14}Ce^{IV}(GaW_{11}O_{39})_2{\cdot}22H_2O$, crystallizes in monoclinic space group $P2_1/n$ with a V of 9739.9(3) Å^3. See Table S4 for more information.

Undecagermanotungstate (GeW_{11}) Complexes. Lastly, the $M(GeW_{11})_2$ series is based on the $[\alpha\text{-}GeW_{11}O_{39}]^{8-}$ lacunary Keggin, which, like (GaW_{11}), was successfully crystallized with metal cations Sr^{2+}, La^{3+}, Ce^{4+}, and Th^{4+}. Across the reported structures, there are a range of average bond lengths of 1.732−1.745 Å for the Ge−O bond, 2.287−2.297 Å for the W−O^x bond, 1.840−2.040 Å for the W−O^c bond, and 1.626−1.738 Å for the W−O^t bond.

$Sr(GeW_{11})_2$, formulated as $Cs_{14}Sr(GeW_{11}O_{39})_2{\cdot}H_2O$, crystallizes in monoclinic space group $P2_1/n$ with a V of 9904.4(4) Å. $Ba(GeW_{11})_2$, formulated as $Cs_{14}Ba(GeW_{11}O_{39})_2{\cdot}5H_2O$, crystallizes in monoclinic space group $P2_1/n$ with a V of 9879.4(2) Å. $La(GeW_{11})_2$, formulated as $Cs_{13}La(GeW_{11}O_{39})_2{\cdot}15H_2O$, crystallized in monoclinic space group $P2_1/n$ with a V of 9806.8(4) Å. $Ce(GeW_{11})_2$, formulated as $Cs_{12}Ce^{IV}(GeW_{11}O_{39})_2{\cdot}22H_2O$, crystallizes in monoclinic space group $P2_1/n$ with a V of 5175.2(3) Å. $Th(GeW_{11})_2$, fully formulated as $Cs_{12}Th(GeW_{11}O_{39})_2{\cdot}9H_2O$, crystallizes in monoclinic space group $P\bar{1}$ with a V of 4818.4(4) Å^3. See Table S5 for more information.

■ ASSOCIATED CONTENT

Supporting Information

The Supporting Information is available free of charge at https://pubs.acs.org/doi/10.1021/acs.inorgchem.4c02254.

List of new compounds reported in this study and associated CCDC numbers, additional experimental section, crystallography tables, summary of crystallography parameters, POM charge density calculations, additional visualization of structures, and additional references (PDF)

Accession Codes

CCDC 2292381, 2292387, 2292389, 2292399, 2292402, 2311175−2311185, 2311281−2311284, 2311735−2311736, and 2326550−2326552 contain the supplementary crystallographic data for this paper. These data can be obtained free of charge via www.ccdc.cam.ac.uk/data_request/cif, or by emailing data_request@ccdc.cam.ac.uk, or by contacting The Cambridge Crystallographic Data Centre, 12 Union Road, Cambridge CB2 1EZ, UK; fax: +44 1223 336033.

■ AUTHOR INFORMATION

Corresponding Authors

Ian Colliard − *Physical and Life Sciences Directorate, Glenn T. Seaborg Institute, Lawrence Livermore National Laboratory, Livermore, California 94550, United States; Material Sciences Division, Lawrence Livermore National Laboratory, Livermore, California 94550, United States;* orcid.org/0000-0003-1883-1155; Email: Colliard1@LLNL.gov

Gauthier J.-P. Deblonde − *Physical and Life Sciences Directorate, Glenn T. Seaborg Institute, Lawrence Livermore National Laboratory, Livermore, California 94550, United States; Nuclear and Chemical Sciences Division, Lawrence Livermore National Laboratory, Livermore, California 94550, United States;* orcid.org/0000-0002-0825-8714; Email: Deblonde1@LLNL.gov

Complete contact information is available at: https://pubs.acs.org/10.1021/acs.inorgchem.4c02254

Notes

The authors declare no competing financial interest.

https://doi.org/10.1021/acs.inorgchem.4c02254
Inorg. Chem. XXXX, XXX, XXX−XXX

■ ACKNOWLEDGMENTS

This material is based upon work supported by the U.S. Department of Energy, Office of Science, Office of Basic Energy Sciences, Heavy Element Chemistry Program at Lawrence Livermore National Laboratory, under Contract DE-AC52-07NA27344. Release number: LLNL-JRNL-864448.

■ REFERENCES

(1) Keggin, J. F. The Structure and Formula of 12-Phosphotungstic Acid. *Proc. R. Soc. A* **1934**, *144* (851), 75−100.
(2) Sadeghi, O.; Zakharov, L. N.; Nyman, M. Aqueous Formation and Manipulation of the Iron-Oxo Keggin Ion. *Science* **2015**, *347* (6228), 1359−1362.
(3) Hou, Y.; Pang, H.; Gómez-García, C. J.; Ma, H.; Wang, X.; Tan, L. Polyoxometalate Metal−Organic Frameworks: Keggin Clusters Encapsulated into Silver-Triazole Nanocages and Open Frameworks with Supercapacitor Performance. *Inorg. Chem.* **2019**, *58* (23), 16028−16039.
(4) Budych, M. J. W.; Staszak, K.; Bajek, A.; Pniewski, F.; Jastrząb, R.; Staszak, M.; Tylkowski, B.; Wieszczycka, K. The Future of Polyoxymetalates for Biological and Chemical Apllications. *Coord. Chem. Rev.* **2023**, *493*, 215306.
(5) Blasco-Ahicart, M.; Soriano-López, J.; Carbó, J. J.; Poblet, J. M.; Galan-Mascaros, J. R. Polyoxometalate Electrocatalysts Based on Earth-Abundant Metals for Efficient Water Oxidation in Acidic Media. *Nature Chem.* **2018**, *10* (1), 24−30.
(6) Gumerova, N. I.; Rompel, A. Polyoxometalates in Solution: Speciation under Spotlight. *Chem. Soc. Rev.* **2020**, *49* (21), 7568−7601.
(7) Busche, C.; Vilà-Nadal, L.; Yan, J.; Miras, H. N.; Long, D.-L.; Georgiev, V. P.; Asenov, A.; Pedersen, R. H.; Gadegaard, N.; Mirza, M. M.; Paul, D. J.; Poblet, J. M.; Cronin, L. Design and Fabrication of Memory Devices Based on Nanoscale Polyoxometalate Clusters. *Nature* **2014**, *515* (7528), 545−549.
(8) Gaita-Ariño, A.; Luis, F.; Hill, S.; Coronado, E. Molecular Spins for Quantum Computation. *Nat. Chem.* **2019**, *11* (4), 301−309.
(9) Bijelic, A.; Aureliano, M.; Rompel, A. The Antibacterial Activity of Polyoxometalates: Structures, Antibiotic Effects and Future Perspectives. *Chem. Commun.* **2018**, *54* (10), 1153−1169.
(10) Gumerova, N. I.; Rompel, A. Speciation Atlas of Polyoxometalates in Aqueous Solutions. *Science Advances* **2023**, *9* (25), No. eadi0814.
(11) Iijima, J.; Naruke, H.; Sanji, T. Chirality Induction in Crystalline Solids Containing Sandwich-Type $[Ln(A2\text{-}P_2W_{17}O_{61})_2]^{17-}$ Polyoxotungstates and Proline. *Inorg. Chem.* **2018**, *57* (21), 13351−13363.
(12) Breibeck, J.; Gumerova, N. I.; Boesen, B. B.; Galanski, M. S.; Rompel, A. Keggin-Type Polyoxotungstates as Mushroom Tyrosinase Inhibitors - A Speciation Study. *Sci. Rep* **2019**, *9* (1), 5183.
(13) Liu, S.-M.; Zhang, Z.; Li, X.-H.; Jia, H.-J.; Liu, S.-X. Synthesis and Photophysical Properties of Crystalline $[EuW_{10}O_{36}]^{9-}$-Based Polyoxometalates with Lanthanide Ions as Counter Cations. *J. Alloys Compd.* **2018**, *761*, 52−57.
(14) Zheng, K.; Ma, P. Recent Advances in Lanthanide-Based POMs for Photoluminescent Applications. *Dalton Trans.* **2024**, *53* (9), 3949−3958.
(15) Neves, C. S.; Granadeiro, C. M.; Cunha-Silva, L.; Ananias, D.; Gago, S.; Feio, G.; Carvalho, P. A.; Eaton, P.; Balula, S. S.; Pereira, E. Europium Polyoxometalates Encapsulated in Silica Nanoparticles − Characterization and Photoluminescence Studies. *Eur. J. Inorg. Chem.* **2013**, *2013* (16), 2877−2886.
(16) Talbot-Eeckelaers, C.; Pope, S. J. A.; Hynes, A. J.; Copping, R.; Jones, C. J.; Taylor, R. J.; Faulkner, S.; Sykes, D.; Livens, F. R.; May, I. Luminescence from Neptunyl(VI) Species in Solution. *J. Am. Chem. Soc.* **2007**, *129* (9), 2442−2443.
(17) Colliard, I.; Lee, J. R. I.; Colla, C. A.; Mason, H. E.; Sawvel, A. M.; Zavarin, M.; Nyman, M.; Deblonde, G. J.-P. Polyoxometalates as Ligands to Synthesize, Isolate and Characterize Compounds of Rare Isotopes on the Microgram Scale. *Nat. Chem.* **2022**, *14* (12), 1357−1366.
(18) Colliard, I.; Deblonde, G. J.-P. Characterization of the First Peacock−Weakley Polyoxometalate Containing a Transplutonium Element: Curium Bis-Pentatungstate $[Cm(W_5O_{18})_2]^{9-}$. *Chem. Commun.* **2024**, *60* (47), 5999−6002.
(19) Nyman, M. Polyoxoniobate Chemistry in the 21st Century. *Dalton Trans.* **2011**, *40* (32), 8049−8058.
(20) Nyman, M.; Burns, P. C. A Comprehensive Comparison of Transition-Metal and Actinyl Polyoxometalates. *Chem. Soc. Rev.* **2012**, *41* (22), 7354−7367.
(21) Misra, A.; Kozma, K.; Streb, C.; Nyman, M. Beyond Charge Balance: Counter-Cations in Polyoxometalate Chemistry. *Angew. Chem., Int. Ed.* **2020**, *59* (2), 596−612.
(22) Ohlin, C. A. Energetics of Paramagnetic Oxide Clusters: The Fe(III) Oxyhydroxy Keggin Ion. *Phys. Chem. Chem. Phys.* **2020**, *22* (7), 4043−4050.
(23) Gorden, A. E. V.; Xu, J.; Raymond, K. N.; Durbin, P. Rational Design of Sequestering Agents for Plutonium and Other Actinides. *Chem. Rev.* **2003**, *103* (11), 4207−4282.
(24) Martin, L. J.; Hähnke, M. J.; Nitz, M.; Wöhnert, J.; Silvaggi, N. R.; Allen, K. N.; Schwalbe, H.; Imperiali, B. Double-Lanthanide-Binding Tags: Design, Photophysical Properties, and NMR Applications. *J. Am. Chem. Soc.* **2007**, *129* (22), 7106−7113.
(25) Özçubukçu, S.; Mandal, K.; Wegner, S.; Jensen, M. P.; He, C. Selective Recognition of Americium by Peptide-Based Reagents. *Inorg. Chem.* **2011**, *50* (17), 7937−7939.
(26) Nash, K. L. The Chemistry of TALSPEAK: A Review of the Science. *Solvent Extr. Ion Exch.* **2015**, *33* (1), 1−55.
(27) Ferrier, M. G.; Stein, B. W.; Bone, S. E.; Cary, S. K.; Ditter, A. S.; Kozimor, S. A.; Lezama Pacheco, J. S.; Mocko, V.; Seidler, G. T. The Coordination Chemistry of CmIII, AmIII, and AcIII in Nitrate Solutions: An Actinide L3-Edge EXAFS Study. *Chem. Sci.* **2018**, *9* (35), 7078−7090.
(28) Tian, G.; Shuh, D. K. A Spectrophotometric Study of Am(III) Complexation with Nitrate in Aqueous Solution at Elevated Temperatures. *Dalton Trans* **2014**, *43* (39), 14565−14569.
(29) Solola, L. A.; Zabula, A. V.; Dorfner, W. L.; Manor, B. C.; Carroll, P. J.; Schelter, E. J. Cerium(IV) Imido Complexes: Structural, Computational, and Reactivity Studies. *J. Am. Chem. Soc.* **2017**, *139* (6), 2435−2442.
(30) Piro, N. A.; Robinson, J. R.; Walsh, P. J.; Schelter, E. J. The Electrochemical Behavior of Cerium(III/IV) Complexes: Thermodynamics, Kinetics and Applications in Synthesis. *Coord. Chem. Rev.* **2014**, *260*, 21−36.
(31) Thakur, P.; Conca, J. L.; Van De Burgt, L. J.; Choppin, G. R. Complexation and the Laser Luminescence Studies of Eu(III), Am(III), and Cm(III) with EDTA, CDTA, and PDTA and Their Ternary Complexation with Dicarboxylates. *J. Coord. Chem.* **2009**, *62* (23), 3719−3737.
(32) Griffiths, T. L.; Martin, L. R.; Zalupski, P. R.; Rawcliffe, J.; Sarsfield, M. J.; Evans, N. D. M.; Sharrad, C. A. Understanding the Solution Behavior of Minor Actinides in the Presence of EDTA4−, Carbonate, and Hydroxide Ligands. *Inorg. Chem.* **2013**, *52* (7), 3728−3737.
(33) Boukhalfa, H.; Reilly, S. D.; Neu, M. P. Complexation of Pu(IV) with the Natural Siderophore Desferrioxamine B and the Redox Properties of Pu(IV)(Siderophore) Complexes. *Inorg. Chem.* **2007**, *46* (3), 1018−1026.
(34) Whisenhunt, D. W.; Neu, M. P.; Hou, Z.; Xu, J.; Hoffman, D. C.; Raymond, K. N. Specific Sequestering Agents for the Actinides. 29. Stability of the Thorium(IV) Complexes of Desferrioxamine B (DFO) and Three Octadentate Catecholate or Hydroxypyridinonate DFO Derivatives: DFOMTA, DFOCAMC, and DFO-1,2-HOPO. Comparative Stability of the Plutonium(IV) DFOMTA Complex1. *Inorg. Chem.* **1996**, *35* (14), 4128−4136.
(35) Evers, A.; Hancock, R. D.; Martell, A. E.; Motekaitis, R. J. Metal Ion Recognition in Ligands with Negatively Charged Oxygen Donor Groups. Complexation of Iron(III), Gallium(III), Indium(III), Aluminum(III), and Other Highly Charged Metal Ions. *Inorg. Chem.* **1989**, *28* (11), 2189−2195.

https://doi.org/10.1021/acs.inorgchem.4c02254
Inorg. Chem. XXXX, XXX, XXX−XXX

(36) Brown, M. A.; Paulenova, A.; Gelis, A. V. Aqueous Complexation of Thorium(IV), Uranium(IV), Neptunium(IV), Plutonium(III/IV), and Cerium(III/IV) with DTPA. *Inorg. Chem.* **2012**, *51* (14), 7741−7748.
(37) Grimes, T. S.; Nash, K. L. Acid Dissociation Constants and Rare Earth Stability Constants for DTPA. *J. Solution Chem.* **2014**, *43* (2), 298−313.
(38) Thiele, N. A.; Brown, V.; Kelly, J. M.; Amor-Coarasa, A.; Jermilova, U.; MacMillan, S. N.; Nikolopoulou, A.; Ponnala, S.; Ramogida, C. F.; Robertson, A. K. H.; Rodríguez-Rodríguez, C.; Schaffer, P.; Williams, Jr. C.; Babich, J. W.; Radchenko, V.; Wilson, J. J. An Eighteen-Membered Macrocyclic Ligand for Actinium-225 Targeted Alpha Therapy. *Angew. Chem., Int. Ed.* **2017**, *56* (46), 14712−14717.
(39) Hu, A.; Wilson, J. J. Advancing Chelation Strategies for Large Metal Ions for Nuclear Medicine Applications. *Acc. Chem. Res.* **2022**, *55*, 904.
(40) Deblonde, G. J.-P.; Mattocks, J. A.; Dong, Z.; Wooddy, P. T.; Cotruvo, J. A.; Zavarin, M. Capturing an Elusive but Critical Element: Natural Protein Enables Actinium Chemistry. *Science Advances* **2021**, *7* (43), No. eabk0273.
(41) Simms, M. E.; Sibley, M. M.; Driscoll, D. M.; Kertesz, V.; Damron, J. T.; Ivanov, A. S.; White, F. D.; Thiele, N. A. Reining in Radium for Nuclear Medicine: Extra-Large Chelator Development for an Extra-Large Ion. *Inorg. Chem.* **2023**, *62* (50), 20834−20843.
(42) White, F. D.; Thiele, N. A.; Simms, M. E.; Cary, S. K. Structure and Bonding of a Radium Coordination Compound in the Solid State. *Nat. Chem.* **2024**, *16* (2), 168−172.
(43) Bai, Z.; Brannon, J.; Celis-Barros, C.; Beck, N.; Sperling, J. M.; Rotermund, B. M.; Martinez, D. G.; Wineinger, H. B.; Albrecht-Schönzart, T. E. Radium Revisited: Revitalization of the Coordination Chemistry of Nature's Largest + 2 Cation. *Inorg. Chem.* **2023**, *62* (22), 8478−8481.
(44) Thiele, N. A.; MacMillan, S. N.; Wilson, J. J. Rapid Dissolution of $BaSO_4$ by Macropa, an 18-Membered Macrocycle with High Affinity for Ba2+. *J. Am. Chem. Soc.* **2018**, *140* (49), 17071−17078.
(45) Kovács, A. Theoretical Study of Actinide Complexes with Macropa. *ACS Omega* **2020**, *5* (41), 26431−26440.
(46) Deblonde, G. J.-P.; Kelley, M. P.; Su, J.; Batista, E. R.; Yang, P.; Booth, C. H.; Abergel, R. J. Spectroscopic and Computational Characterization of Diethylenetriaminepentaacetic Acid/Transplutonium Chelates: Evidencing Heterogeneity in the Heavy Actinide(III) Series. *Angew. Chem., Int. Ed.* **2018**, *57* (17), 4521−4526.
(47) Polinski, M. J.; Garner, E. B.; Maurice, R.; Planas, N.; Stritzinger, J. T.; Parker, T. G.; Cross, J. N.; Green, T. D.; Alekseev, E. V.; Van Cleve, S. M.; Depmeier, W.; Gagliardi, L.; Shatruk, M.; Knappenberger, K. L.; Liu, G.; Skanthakumar, S.; Soderholm, L.; Dixon, D. A.; Albrecht-Schmitt, T. E. Unusual Structure, Bonding and Properties in a Californium Borate. *Nat. Chem.* **2014**, *6* (5), 387−392.
(48) Silver, M. A.; Cary, S. K.; Johnson, J. A.; Baumbach, R. E.; Arico, A. A.; Luckey, M.; Urban, M.; Wang, J. C.; Polinski, M. J.; Chemey, A.; Liu, G.; Chen, K.-W.; Van Cleve, S. M.; Marsh, M. L.; Eaton, T. M.; van de Burgt, L. J.; Gray, A. L.; Hobart, D. E.; Hanson, K.; Maron, L.; Gendron, F.; Autschbach, J.; Speldrich, M.; Kögerler, P.; Yang, P.; Braley, J.; Albrecht-Schmitt, T. E. Characterization of Berkelium(III) Dipicolinate and Borate Compounds in Solution and the Solid State. *Science* **2016**, *353* (6302), ZZZ.
(49) Leguay, S.; Vercouter, T.; Topin, S.; Aupiais, J.; Guillaumont, D.; Miguirditchian, M.; Moisy, P.; Le Naour, C. New Insights into Formation of Trivalent Actinides Complexes with DTPA. *Inorg. Chem.* **2012**, *51* (23), 12638−12649.
(50) Huffman, Z. K.; Sperling, J. M.; Windorff, C. J.; Long, B. N.; Cordova, L.; Ramanantoanina, H.; Celis-Barros, C.; Albrecht-Schönzart, T. E. Synthesis and Characterization of a Bimetallic Americium(III) Pyrithionate Coordination Complex. *Chem. Commun.* **2022**, *58* (84), 11791−11794.
(51) Colla, C. A.; Colliard, I.; Sawvel, A. M.; Nyman, M.; Mason, H. E.; Deblonde, G. J.-P. Contrasting Trivalent Lanthanide and Actinide Complexation by Polyoxometalates via Solution-State NMR. *Inorg. Chem.* **2023**, *62* (16), 6242−6254.
(52) Colliard, I.; Deblonde, G. J.-P. Polyoxometalate Ligands Reveal Different Coordination Chemistries Among Lanthanides and Heavy Actinides. *JACS Au* **2024**, *4* (7), 2503−2513.
(53) Pope, M. T. *Heteropoly and Isopoly Oxometalates*, 1st ed.; Inorganic Chemistry Concepts; Springer: Berlin, 1983.
(54) Iijima, J.; Ishikawa, E.; Nakamura, Y.; Naruke, H. Synthesis and Structural Investigation of Sandwich Polyoxotungstates Containing Cerium (III/IV) and Mono-Lacunary Keggin Tungstophosphate Units. *Inorg. Chim. Acta* **2010**, *363* (7), 1500−1506.
(55) Falaise, C.; Mpacko Priso, G.; Leclerc, N.; Haouas, M.; Cadot, E. Making Heterometallic Metal−Metal Bonds in Keggin-Type Polyoxometalates by a Six-Electron Reduction Process. *Inorg. Chem.* **2023**, *62* (6), 2494−2502.
(56) Sousa, F. L.; Pillinger, M.; Sá Ferreira, R. A.; Granadeiro, C. M.; Cavaleiro, A. M. V.; Rocha, J.; Carlos, L. D.; Trindade, T.; Nogueira, H. I. S. Luminescent Polyoxotungstoeuropate Anion-Pillared Layered Double Hydroxides. *Eur. J. Inorg. Chem.* **2006**, *2006* (4), 726−734.
(57) Mougharbel, A. S.; Bhattacharya, S.; Bassil, B. S.; Rubab, A.; van Leusen, J.; Kögerler, P.; Wojciechowski, J.; Kortz, U. Lanthanide-Containing 22-Tungsto-2-Germanates $[Ln(GeW_{11}O_{39})_2]^{13-}$: Synthesis, Structure, and Magnetic Properties. *Inorg. Chem.* **2020**, *59* (7), 4340−4348.
(58) Pope, M. T.; Müller, A. Polyoxometalate Chemistry: An Old Field with New Dimensions in Several Disciplines. *Angewandte Chemie International Edition in English* **1991**, *30* (1), 34−48.
(59) Zhang, C.; Howell, R. C.; Scotland, K. B.; Perez, F. G.; Todaro, L.; Francesconi, L. C. Aqueous Speciation Studies of Europium(III) Phosphotungstate. *Inorg. Chem.* **2004**, *43* (24), 7691−7701.
(60) Kholdeeva, O. A.; Maksimov, G. M.; Maksimovskaya, R. I.; Vanina, M. P.; Trubitsina, T. A.; Naumov, D. Yu.; Kolesov, B. A.; Antonova, N. S.; Carbó, J. J.; Poblet, J. M. ZrIV-Monosubstituted Keggin-Type Dimeric Polyoxometalates: Synthesis, Characterization, Catalysis of H_2O_2-Based Oxidations, and Theoretical Study. *Inorg. Chem.* **2006**, *45* (18), 7224−7234.
(61) Tourné, C. M.; Tourné, G. F.; Brianso, M.-C. Bis-(undecatungstogermanato)uranate(IV) de césium: $Cs_{12}[U(GeW_{11}O_{39})_2].13-14H_2O$. *Acta Cryst. B* **1980**, *36* (9), 2012−2018.
(62) Cai, L.; Li, Y.; Yu, C.; Ji, H.; Liu, Y.; Liu, S. Spontaneous Resolution of a Chiral Polyoxometalate: Synthesis, Crystal Structures and Properties. *Inorg. Chim. Acta* **2009**, *362* (8), 2895−2899.
(63) Shannon, R. D. Revised Effective Ionic Radii and Systematic Studies of Interatomie Distances in Halides and Chaleogenides. *Acta crystallographica* **1976**, *A32*, 751−767.
(64) Kato, C. N.; Shinohara, A.; Hayashi, K.; Nomiya, K. Syntheses and X-Ray Crystal Structures of Zirconium(IV) and Hafnium(IV) Complexes Containing Monovacant Wells−Dawson and Keggin Polyoxotungstates. *Inorg. Chem.* **2006**, *45* (20), 8108−8119.
(65) Antonio, M. R.; Nyman, M.; Anderson, T. M. Direct Observation of Contact Ion-Pair Formation in Aqueous Solution. *Angew. Chem., Int. Ed.* **2009**, *48* (33), 6136−6140.
(66) Weinstock, I. A.; Cowan, J. J.; Barbuzzi, E. M. G.; Zeng, H.; Hill, C. L. Equilibria between α and β Isomers of Keggin Heteropolytungstates. *J. Am. Chem. Soc.* **1999**, *121* (19), 4608−4617.
(67) Tézé, A.; Michelon, M.; Hervé, G. Syntheses and Structures of the Tungstoborate Anions. *Inorg. Chem.* **1997**, *36* (4), 505−509.

https://doi.org/10.1021/acs.inorgchem.4c02254
Inorg. Chem. XXXX, XXX, XXX−XXX